Eur. Phys. J. E (2021) 44:19
https://doi.org/10.1140/epje/s10189-021-00019-8

THE EUROPEAN PHYSICAL JOURNAL E

Regular Article - Living Systems

Modelling the effect of ribosome mobility on the rate of protein synthesis

Olivier Dauloudet[1,2], Izaak Neri[3,a], Jean-Charles Walter[1,b], Jérôme Dorignac[1], Frédéric Geniet[1], and Andrea Parmeggiani[1,2,c]

[1] Laboratoire Charles Coulomb (L2C), CNRS, Montpellier University, Montpellier, France
[2] Laboratory of Parasite Host Interactions (LPHI), CNRS, Montpellier University, Montpellier, France
[3] Department of Mathematics, King's College London, Strand, London WC2R 2LS, UK

Received 30 September 2020 / Accepted 15 January 2021 / Published online 8 March 2021

Abstract Translation is one of the main steps in the synthesis of proteins. It consists of ribosomes that translate sequences of nucleotides encoded on mRNA into polypeptide sequences of amino acids. Ribosomes bound to mRNA move unidirectionally, while unbound ribosomes diffuse in the cytoplasm. It has been hypothesized that finite diffusion of ribosomes plays an important role in ribosome recycling and that mRNA circularization enhances the efficiency of translation, see e.g. Lodish et al. (Molecular cell biology, 8th edn, W.H. Freeman and Company, San Francisco, 2016). In order to estimate the effect of cytoplasmic diffusion on the rate of translation, we consider a totally asymmetric simple exclusion process coupled to a finite diffusive reservoir, which we call the ribosome transport model with diffusion. In this model, we derive an analytical expression for the rate of protein synthesis as a function of the diffusion constant of ribosomes, which is corroborated with results from continuous-time Monte Carlo simulations. Using a wide range of biological relevant parameters, we conclude that diffusion is not a rate limiting factor in translation initiation because diffusion is fast enough in biological cells.

1 Introduction

Cells synthesize proteins by first transcribing the hereditary information encoded in genes into functional mRNA and subsequently by translating the mRNA nucleotide sequence into polypeptide sequences [1]. The translation of mRNA into a polypeptide sequence can be divided into three stages, namely the initiation, elongation and termination stages [1]. During initiation, a ribosomal complex (consisting of two ribosomal subunits, initiation factors, and tRNA) is assembled at the 5' end of a mRNA chain. After initiation, the ribosomal complex moves (or elongates) from the 5' end towards the 3' end of the mRNA while forming a polypeptide chain. In the final termination stage, the ribosome complex releases the polypeptide chain, unbinds from the mRNA and disassembles.

Translation is mainly controlled at the initiation step, as it is the rate limiting step in translation [2–5]. Initiation is a complex process involving several molecular actors, and it is therefore difficult to understand all the molecular mechanisms that are relevant for translation control. Nevertheless, coarse-grained mathematical modelling can uncover which physical mechanisms play a role in translation control.

It has been argued that the recycling of ribosomes through Brownian diffusion in the cytosol plays an important role in the control or regulation of translation [1,6–8]. When a ribosome unbinds from the mRNA after termination, it can either rebind to the same mRNA or bind to another mRNA. If the diffusion of ribosomes is slow enough, then circularization of the mRNA could enhance the rate of ribosome recycling through cytosolic diffusion [1,6,9,10]. On the other hand, this effect would be negligible if diffusion of ribosomes is fast enough. In this paper, we use physical modelling to determine whether recycling of ribosomes through diffusion can play a role in controlling mRNA translation.

In order to study how ribosome mobility affects the mRNA initiation rate and thus the protein production, we present a minimalistic physical model that describes both the translation of mRNA by ribosomes and the diffusion of ribosomes in the cytoplasm. We call this model the ribosome transport model with diffusion (RTD). From a physical viewpoint, the RTD consists of particles (the ribosomes) that diffuse in a box and can bind to a one-dimensional substrate (mRNA). Particles bound to the substrate move unidirectionally and cannot overtake. The RTD consists thus in a totally asymmetric simple exclusion process (TASEP) [11] in contact with a diffusive reservoir. If diffusion is fast enough, then we recover the standard TASEP model,

[a] e-mail: izaak.neri@kcl.ac.uk (corresponding author)
[b] e-mail: jean-charles.walter@umontpellier.fr
[c] e-mail: andrea.parmeggiani@umontpellier.fr

which describes in detail the elongation stage of mRNA translation [12–16]. On the other hand, when diffusion is slow, then a concentration gradient is formed in the reservoir and there will be a tight coupling between active transport on the filament and diffusion in the reservoir. In this regime, the RTD describes the interplay of active and passive transport in cellular media, leading to the formation of a gradient of molecular species. Phenomena of active transport coupled to a diffusive reservoir have been studied before in the literature, see, for example, Refs. [6–8,17–28]. In these studies, much focus has been put on nonequilibrium phase transitions [11,22,29,30].

In the present paper, we use mean-field theory to derive an analytical expression for the protein synthesis in the RTD model, which is corroborated with numerical results obtained from continuous-time Monte Carlo simulations. Subsequently, we use the analytical expression for the protein synthesis rate to discuss the biological relevance of Brownian diffusion in ribosomal recycling. By considering a broad range of biological parameters, we come to the conclusion that under physiological conditions finite diffusion of ribosomes is not important in the control of mRNA translation. Thus, circularisation should not occur in order to prevent the limiting effect of Brownian diffusion of ribosomes in the cytoplasm on initiation of translation [1,6,9,10]. In addition, we discuss how the spatial dimensions of the reservoir and geometry impact the protein synthesis rate and we find qualitative difference in the dependence of the protein synthesis rate on the length of the mRNA between two and three dimensions. Both cases are biologically relevant: the three-dimensional case applies to cytoplasmic translation, whereas the two-dimensional case applies to endoplasmic reticulum translation.

The paper is organized as follows. In Sect. 2, we define the RTD model. In Sect. 3, we present a mean-field theory for the RTD model and derive analytical expressions for the protein synthesis rate as a function of the diffusion coefficient of ribosomes. In Sect. 4, we compare theory with simulations results using a continuous-time algorithm. In Sect. 5, we discuss the biological relevance of the model. We conclude the paper with a discussion in Sect. 6, and in Appendix A we present analytical results for the concentration profile of ribosomes in the cytoplasm.

2 Model definition: Ribosome Transport with Diffusion

We introduce here the RTD, a minimalistic model that allows us to study how diffusion determines the rate of protein synthesis. The RTD consists of ribosomes that diffuse in a medium embedded in two or three dimensions and can bind to a one-dimensional substrate, say a mRNA filament. Bound ribosomes then move unidirectionally along the filament by converting the intracellular chemical energy from the hydrolysis of guanine triphosphate (GTP) into mechanical motion, which is modelled by a totally asymmetric simple exclusion process (TASEP). In Fig. 1, we present an illustration of the model and its parameters.

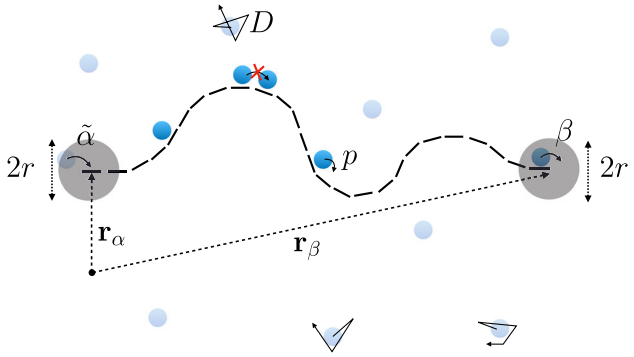

Fig. 1 Graphical illustration of the ribosome transport with diffusion model (RTD). The mRNA is represented with a dashed line, ribosomes processing along the mRNA at a rate p are represented by dark blue discs, and ribosomes diffusing freely at a diffusion coefficient D are represented by light blue discs. Grey discs of radius r centred at the end-point of the mRNA are the reaction volumes: if a diffusing ribosome is located in the reaction volume at the mRNA end-point centred around position $\mathbf{r}_\alpha$, then it attaches at a rate $\tilde{\alpha}$ to the mRNA. On the other hand, if a ribosome is at the last site of the mRNA, then it detaches at a rate β and is released inside the reaction volume centred around $\mathbf{r}_\beta$

We consider a filament immersed in a medium containing ribosomes at a concentration c_∞. The filament is a homopolymer consisting of ℓ monomers of length a. The first and last monomers of the filament are located at positions $\mathbf{r}_\alpha$ and $\mathbf{r}_\beta$, respectively. For simplicity, we consider that $\mathbf{r}_\alpha$ and $\mathbf{r}_\beta$ are fixed in time.

The dynamics of unbound molecular motors is modelled as a Brownian motion with diffusion coefficient D.

The dynamics of bound molecular motors is a unidirectional, hopping process with excluded volume interactions, which we model with a TASEP on a one-dimensional lattice of length $L = \ell a$ [12,13,29,30]. The TASEP model is a Markov jump process with the following rates: the hopping (or elongation) rate p at which particles make a step of length a, the exit rate β at which particles detach from the filament end-point, and the entry rate

$$\alpha(t) = \tilde{\alpha}\, N_{\mathrm{r}}(t), \tag{1}$$

where $\tilde{\alpha}$ is the rate at which ribosomes contained in the reaction volume bind to the filament and $N_{\mathrm{r}}(t)$ is the number of ribosomes present in the reaction volume at time t. The reaction volume is considered to be a sphere (in three dimensions) or a disc (in two dimensions) of radius r centred around the first monomer of the filament located at $\mathbf{r}_\alpha$. The reaction volume radius is of the same order of magnitude as the size of a ribosome. When ribosomes detach from the filament, they appear at a random location in a sphere (in

three dimensions) or disc (in two dimensions) of radius r centred around $\mathbf{r}_\beta$. Because of excluded volume interactions, each monomer can be bound to at most one ribosome. Therefore, ribosomes cannot hop forward if the subsequent monomer is already occupied by a ribosome and ribosomes cannot bind to the first monomer when it is already occupied, as illustrated in Fig. 1.

3 Mean-field theory for coupling of diffusion with active transport

We present a mean field theory for the RTD model that couples diffusion with active transport. First, in Sect. 3.1, we discuss how the protein synthesis rate is related to the stationary current of the TASEP model. Second, in Sect. 3.2, we derive an analytical expression for the protein synthesis rate that is independent of the geometrical properties of the medium or reservoir in which the one-dimensional substrate is immersed, in the sense that the geometrical aspect of the problem is captured in the value of one nonuniversal constant. Lastly, in Sect. 3.3, we discuss the impact of the geometry of the surrounding reservoir on the protein synthesis rate.

3.1 Protein synthesis rate is given by the stationary current on the filament

The quantity of interest from a biological point of view is the protein synthesis rate J, which corresponds with the stationary current of particles on the filament [12, 13].

The stationary current of the RTD model in the limit of infinitely large D is equal to the stationary current $\mathcal{J}$ of the TASEP model. In the limit of large ℓ, it holds that [11,29,31]

$$\mathcal{J} = \begin{cases} \alpha\left(1-\frac{\alpha}{p}\right), & \alpha<\beta \text{ and } \alpha<p/2, \quad \text{(LD)},\\ \beta\left(1-\frac{\beta}{p}\right), & \beta<\alpha \text{ and } \beta<p/2, \quad \text{(HD)},\\ \frac{p}{4}, & \alpha\geq p/2 \text{ and } \beta\geq p/2, \quad \text{(MC)}. \end{cases} \tag{2}$$

The three branches in Eq. (2) correspond with three nonequilibrium phases: a low-density phase (LD) at small entry rates $\alpha<\beta$ and $\alpha<p/2$, a high-density phase (HD) at small exit rates $\beta<\alpha$ and $\beta<p/2$, and a maximal current phase (MC) when both $\alpha\geq p/2$ and $\beta\geq p/2$. In the LD phase, the ribosome attachment process is rate limiting and the current is a function of α; in the HD phase, the ribosome detachment process is rate limiting and the current is a function of β; and in the MC phase, the filament hopping process is rate limiting and the current is independent of both α and β. Experimental data in yeast cells [32] and in neurons of mammals [33] show that the rate limiting process for translation is the initiation of ribosomes.

In the RTD model at finite values of D, the entry rate $\alpha(t)$ on the filament is not a constant but a fluctuating quantity, see Eq. (1). In the stationary state, the average current J is well approximated by the expression (2) with the entry rate α replaced by its average value

$$\langle\alpha(t)\rangle = \tilde{\alpha}\,\langle N_{\mathrm{r}}(t)\rangle, \tag{3}$$

where $\langle\cdot\rangle$ denotes the average over many realizations of the stationary process. Since in the stationary state the average number $\langle N_{\mathrm{r}}(t)\rangle$ of ribosomes in the reaction volume is independent of time, we set

$$\langle\alpha(t)\rangle = \langle\alpha\rangle. \tag{4}$$

Replacing in Eq. (2) α by $\langle\alpha\rangle$, we obtain for the stationary current of the RTD model the expression

$$J = \begin{cases} \langle\alpha\rangle\left(1-\frac{\langle\alpha\rangle}{p}\right), & \langle\alpha\rangle<\beta \text{ and } \langle\alpha\rangle<p/2, \quad \text{(LD)},\\ \beta\left(1-\frac{\beta}{p}\right), & \beta<\langle\alpha\rangle \text{ and } \beta<p/2, \quad \text{(HD)},\\ \frac{p}{4}, & \langle\alpha\rangle\geq p/2 \text{ and } \beta\geq\frac{p}{2}, \quad \text{(MC)}. \end{cases} \tag{5}$$

Note that replacing α by $\langle\alpha\rangle$ is a mean-field approximation because it neglects correlations between particles in the reaction volume and particles on the filament. From Eq. (5), we observe that if the filament is in the HD or MC phase, then the protein synthesis rate is independent of the diffusion process in the reservoir. However, in the LD phase when the initiation step is rate limiting, which is the biologically relevant case, the current J depends on the concentration of unbound ribosomes through $\langle\alpha\rangle$, and hence in this regime we are required to include diffusion into our theoretical analysis. Often it will be insightful to consider the limiting case where particle excluded volume on the filament is irrelevant for which the simpler formula

$$J = \langle\alpha\rangle \tag{6}$$

holds. Note that this condition is fulfilled for low density of ribosomes on the filament.

3.2 Protein synthesis rate: universal expression

From the point of view of the reservoir of diffusing ribosomes, the filament serves both as a sink and a source of ribosomes.

If the initiation and termination sites overlap, as will be approximately the case for circular mRNA, then the concentration of ribosomes in the reservoir will be homogeneous since source and sink exactly compensate for each other, and therefore in this case

$$\langle\alpha\rangle = \alpha_\infty = \tilde{\alpha}c_\infty\mathcal{V}, \tag{7}$$

where $\mathcal{V}$ is the reaction volume of radius r, which for two dimensions and three dimensions is given by $\mathcal{V}=\pi r^2$ and $\mathcal{V}=4\pi r^3/3$, respectively.

On the other hand, if the termination site is distant from the initiation site, then $\langle\alpha\rangle$ will have a reduced value, with respect to Eq. (7) due to the depletion of

ribosomes in the reaction volume at the initiation site. Indeed, the current on the filament carries away ribosomes from the reaction volume, which in the stationary state will be compensated by the diffusive current in the reservoir. As we will show in the next section, the depletion effects due to finite diffusion are captured by the formula

$$\langle\alpha\rangle = \alpha_\infty \left(1 - \frac{J\mu_d}{D_{\rm eff}\alpha_\infty}\right), \tag{8}$$

where μ_d is a constant that depends on the geometry of the problem and where

$$D_{\rm eff} = \frac{D}{\tilde{\alpha} r^2} \tag{9}$$

is an effective diffusion coefficient. The dimensionless quantity $D_{\rm eff}$ quantifies the competition between injection of ribosomes on the filament and the diffusion of ribosomes into the reaction volume. Equation (8) follows from solving the diffusion equation for ribosomes in the reservoir, as we shall describe in detail in the next section. Equation (8) states that the rate $\langle\alpha\rangle$ is the sum of the entry rate α_∞ for a homogeneous reservoir minus a correction term that captures the effect of finite diffusion on the entry rate. The correction term is negative since the filament depletes particles in the reaction volume at the initiation site. Moreover, Eq. (8) states that the correction term is proportional to the current J on the filament, inversely proportional to the effective diffusion constant $D_{\rm eff}$, and it is also proportional to the dimensionless, nonuniversal constant μ_d that depends, as we shall see in the next section, on the geometrical properties of the system, namely, the end-to-end distance $|\mathbf{r}_\beta - \mathbf{r}_\alpha|$, the location of the filament in the reservoir, the dimensionality of the system, and the boundary conditions of the reservoir of diffusing ribosomes. Here, we would like to focus on the physical consequences of Eqs. (8) and (9).

To obtain the protein synthesis rate J, we combine Eqs. (5) and (8). In the LD phase, we obtain a second-order algebraic equation whose solution $\langle\alpha\rangle \in [0, p/2]$ is given by

$$\langle\alpha\rangle = p\frac{D_{\rm eff}+\mu_d}{2\mu_d}\left(1 - \sqrt{1-4\zeta}\right), \tag{10}$$

where the adimensional parameter

$$\zeta = \frac{\alpha_\infty D_{\rm eff}\mu_d}{p(D_{\rm eff}+\mu_d)^2} \tag{11}$$

quantifies the effect of exclusion on $\langle\alpha\rangle$. The argument of the square root in (10) is always positive when the filament is in the LD phase because in the LD phase $\alpha_\infty < p/2(1+\mu_d/(2D_{\rm eff}))$, which implies $\zeta < 1/4$. Note that if the diffusion coefficient $D_{\rm eff}$ is small enough, then $\zeta \ll 1/4$ and exclusion has a minor effect. Plugging $\langle\alpha\rangle$ inside the expression for the current, given by Eq. (5), we obtain the following expression for the protein synthesis rate,

$$J = \begin{cases} \langle\alpha\rangle\left(1-\langle\alpha\rangle/p\right), & \alpha_\infty < \beta\left[1+\frac{\mu_d}{D_{\rm eff}}(1-\beta/p)\right] \\ & \text{and } \alpha_\infty < p/2\left(1+\frac{\mu_d}{2D_{\rm eff}}\right), \quad \text{(LD)}, \\ \beta\left(1-\frac{\beta}{p}\right), & \alpha_\infty > \beta\left[1+\frac{\mu_d}{D_{\rm eff}}(1-\beta/p)\right] \\ & \text{and } \beta < p/2, \quad \text{(HD)}, \\ \frac{p}{4}, & \alpha_\infty \geq p/2\left(1+\frac{\mu_d}{2D_{\rm eff}}\right) \\ & \text{and } \beta \geq p/2, \quad \text{(MC)}, \end{cases} \tag{12}$$

where $\langle\alpha\rangle$ is given by (10). For small values of ζ, the filament will be in the LD phase, and we obtain the simpler expression

$$J = \frac{\alpha_\infty D_{\rm eff}}{D_{\rm eff}+\mu_d}, \tag{13}$$

which also follows from Eq. (6). Equation (12) implies that the current J admits a universal expression that only depends on four parameters: the entry rate α_∞ for a homogeneous reservoir, the elongation rate p, the exit rate β, and the parameter $\mu_d/D_{\rm eff}$ that quantifies the effect of finite diffusion on the current J. From Eqs. (12) and (13), it also follows that the effect of finite mobility of ribosomes on the protein synthesis rate J is significant when $\mu_d \gg D_{\rm eff}$. On the other hand, when $\mu_d \ll D_{\rm eff}$, then the finite mobility of ribosomes will be irrelevant for J.

In Fig. 2a, we present the phase diagram for the RTD model for three values of $\mu_d/D_{\rm eff}$, namely the case with an infinite diffusion rate, $\mu_d/D_{\rm eff} = 0$, and two cases with finite diffusion rates, $\mu_d = D_{\rm eff}$ and $\mu_d = 5D_{\rm eff}$. For $\mu_d/D_{\rm eff} = 0$, we recover the phase diagram of TASEP [11,29,31], while for finite values of μ_d we observe an increase of the LD phase and a corresponding decrease of the MC and HD phases. This is because finite diffusion depletes particles in the reaction volume surrounding the initiation site of the filament, and hence reduces the current on the filament for a given α_∞. This is shown in Fig. 2b, where we plot the current as a function of α_∞/p for a fixed value of $\mu_d/D_{\rm eff}$ and $\beta/p \geq 1/2$. If $\mu_d \ll D_{\rm eff}$, then the reservoir is homogeneous and we obtain the standard TASEP result [11,29,31]

$$J = \begin{cases} \alpha_\infty(1-\alpha_\infty/p), & \alpha_\infty < p/2, \\ p/4, & \alpha_\infty > p/2. \end{cases} \tag{14}$$

In the opposing limiting case when $\mu_d \gg D_{\rm eff}$, the reservoir is strongly inhomogeneous and we obtain that

$$J = \begin{cases} \frac{D_{\rm eff}\alpha_\infty}{\mu_d}, & \alpha_\infty < p\mu_d/4, \\ p/4, & \alpha_\infty > p\mu_d/4. \end{cases} \tag{15}$$

In this limit, the environment is viscous and therefore the effects of excluded volume become negligible.

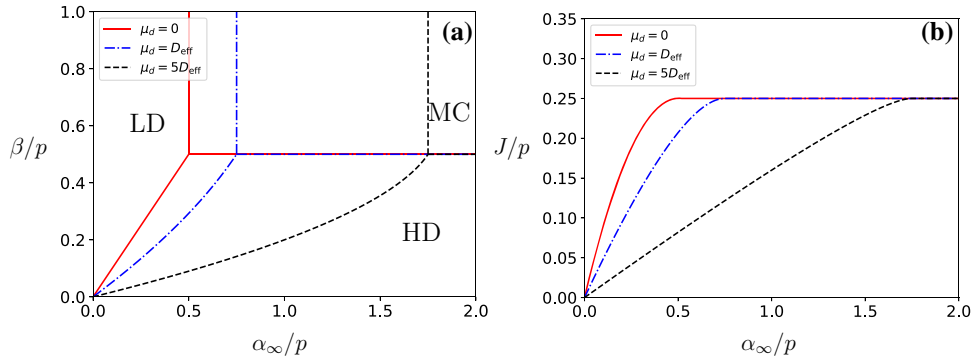

Fig. 2 **a** Phase diagram for the RTD model for three values of the parameter μ_d/D_{eff}. **b** Protein synthesis rate J/p in the RTD model as a function of the ratio α_∞/p for a large exit rate $\beta > p/2$

Note that the results of Fig. 2 do not consider the effects of finite resources. Therefore, it is implicitly assumed that the number of ribosomes is very large compared to the average number of ribosomes on the mRNA. In the case of finite resources, the phase diagram displays an extended shock phase, as shown in Refs. [27,34].

So far, much of the interesting physics has been hidden in the dimensionless constant μ_d that depends on the geometry of the problem. In the next subsection, we will explicitly solve the diffusion equation coupled to directed transport on the filament to obtain explicit expressions for μ_d.

3.3 Influence of geometry on the protein synthesis rate

In order to obtain an expression for μ_d, and thus complete the theoretical treatment for ribosomes with finite mobility, we solve the diffusion equation in the reservoir coupled with active transport on the filament. We consider the case where $|\mathbf{r}_\beta - \mathbf{r}_\alpha| > 2r$ so that the reaction volumes at the source and the sink do not overlap.

The concentration $c(\mathbf{r}, t)$ of unbound ribosomes at the spatial coordinate $\mathbf{r} \in \mathbb{R}^d$ and at the time t is described by the diffusion equation:

$$\frac{\partial c(\mathbf{r},t)}{\partial t} = -\vec{\nabla} \cdot \vec{J}_d(\mathbf{r},t) - \Pi(\mathbf{r},t), \tag{16}$$

where

$$\vec{J}_d(\mathbf{r},t) = -D\vec{\nabla} c(\mathbf{r},t) \tag{17}$$

is the diffusive current, and

$$\Pi(\mathbf{r}) = \begin{cases} \frac{J}{\mathcal{V}} & |\mathbf{r}-\mathbf{r}_\alpha| \le r, \\ -\frac{J}{\mathcal{V}} & |\mathbf{r}-\mathbf{r}_\beta| \le r, \\ 0 & |\mathbf{r}-\mathbf{r}_\alpha| > r \quad \text{and} \quad |\mathbf{r}-\mathbf{r}_\beta| > r, \end{cases} \tag{18}$$

is proportional to the rate J at which particles exit and enter the filament. We have used that $|\mathbf{r}_\beta - \mathbf{r}_\alpha| > 2r$.

The stationary concentration $c(\mathbf{r})$ of unbound ribosomes solves the Poisson equation

$$D\,\Delta c(\mathbf{r}) = \Pi(\mathbf{r}), \tag{19}$$

where Δ is the Laplacian with respect the radius $\mathbf{r}$.

The Poisson equation admits the solution

$$c(\mathbf{r}) = c_\infty + \int_{\mathbb{R}^d} \mathrm{d}^d\mathbf{r}'\, \mathcal{G}_d(\mathbf{r},\mathbf{r}')\Pi(\mathbf{r}'), \tag{20}$$

where $\mathcal{G}_d(\mathbf{r},\mathbf{r}')$ is the Green function that solves

$$D\Delta\mathcal{G}_d(\mathbf{r},\mathbf{r}') = \delta(\mathbf{r}-\mathbf{r}'). \tag{21}$$

The entry rate $\langle\alpha\rangle$ is related to the stationary concentration in the reaction volume through

$$\langle\alpha\rangle = \tilde{\alpha} \int_{|\mathbf{r}-\mathbf{r}_\alpha|\le r} c(\mathbf{r})\mathrm{d}\mathbf{r}. \tag{22}$$

Note that the latter equation is consistent with Eq. (3) because at the stationary state $\langle N_r(t)\rangle = \int_{|\mathbf{r}-\mathbf{r}_\alpha|\le r} c(\mathbf{r})\,\mathrm{d}\mathbf{r}$.

The explicit form of the Green's function and thus $\langle\alpha\rangle$ depend on the geometry of the reservoir. We provide below a couple of examples.

3.3.1 RTD in two-dimensional infinite box ($\mathbb{R}^2$)

In two dimensions, the Green function takes the form [35,36]

$$\mathcal{G}_2(\mathbf{r},\mathbf{r}') = -\frac{1}{2\pi}\ln|\mathbf{r}-\mathbf{r}'|. \tag{23}$$

Substituting the Green function in Eq. (20), we obtain an explicit expression for $c(\mathbf{r})$, see Appendix A. Subsequently, substituting the explicit solution for $c(\mathbf{r})$ in Eq. (22) we obtain the formula Eq. (8) with

$$\mu_2 = \frac{\log d_{\alpha\beta} + 1}{2}, \tag{24}$$

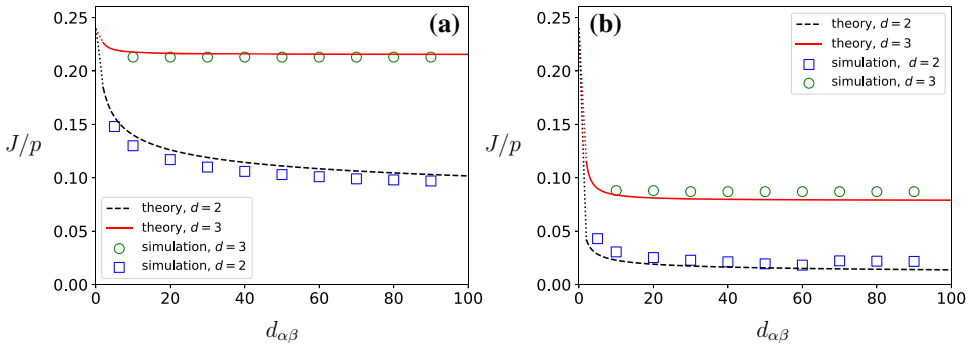

Fig. 3 Protein synthesis rate J/p as a function of the filament end-to-end distance $d_{\alpha\beta}$ for parameters $\alpha_\infty/p = 0.4$, $\beta/p = 1$ for $D_{\text{eff}} = 1$ (**a**) and $D_{\text{eff}} = 0.1$ (**b**). Theoretical result Eq. (12) for filaments in $\mathbb{R}^2$ ($d = 2$, red solid lines) and $\mathbb{R}^3$ ($d = 3$, black dashed lines) is compared with simulations results for filaments consisting of $\ell = 100$ monomers (markers). The theoretical result Eq. (12) applies for $d_{\alpha\beta} > 2$ and $J/p = 0.24$ for $d_{\alpha\beta} = 0$. Therefore, we have added dotted lines connecting $J/p = 0.24$ for $d_{\alpha\beta} = 0$ with J/p at $d_{\alpha\beta} = 2$. The remaining parameters that specify the simulations can be found in Sect. 4

where

$$d_{\alpha\beta} = \frac{|\mathbf{r}_\beta - \mathbf{r}_\alpha|}{r} \tag{25}$$

is the effective distance between the initiation site and the termination site on the filament. Substitution of μ_d into Eqs. (10–12) provides us with an explicit expression for the current J as a function of $d_{\alpha\beta}$.

In Fig. 3, we plot the current J as a function of the separation $d_{\alpha\beta}$ between the two end-points of the mRNA for two values of the effective diffusion constant D_{eff}. Although the part for $d_{\alpha\beta} < 2$ is not covered by our calculations, we know that $J = \alpha_\infty(1 - \alpha_\infty/p)$ for $d_{\alpha\beta} = 0$, which in Fig. 3 corresponds to $J = 0.24p$. We observe that the current decreases monotonically as function of $d_{\alpha\beta}$ and approaches zero for $d_{\alpha\beta}$ large enough. The decay towards zero is logarithmically slow after a fast initial decay in the regime $d_{\alpha\beta} < 2$ where initiation and termination sites overlap.

3.3.2 RTD in three-dimensional infinite box ($\mathbb{R}^3$)

In three dimensions, the Green function is given by

$$\mathcal{G}_3(\mathbf{r}, \mathbf{r}') = \frac{1}{4\pi} \frac{1}{|\mathbf{r} - \mathbf{r}'|}. \tag{26}$$

Using this expression for the Green function in Eq. (20), we obtain an explicit expression for $c(\mathbf{r})$, see Appendix A, which we substitute in Eqs. (20) and (22) to obtain formula Eq. (8) with now

$$\mu_3 = \frac{2}{5} - \frac{1}{3d_{\alpha\beta}}. \tag{27}$$

Comparing Eqs. (24) and (27), we see that there is a difference between two and three dimensions: in three dimensions μ_3 converges to a finite value for $d_{\alpha\beta} \to \infty$ whereas in two dimensions μ_2 diverges for $d_{\alpha\beta} \to \infty$. This implies that in two dimensions J converges to zero for large distances $d_{\alpha\beta}$ between the end-points of the filament, while it converges to a finite nonzero value in three dimensions.

The distinction between the dependency of the current J in two and three dimensions is illustrated in Fig. 3. In three dimensions, the current saturates fast to its asymptotic value after an initial quick decay for values $d_{\alpha\beta} < 2$. The asymptotic value of J depends on the diffusion constant D_{eff} and decreases to zero for $D_{\text{eff}} \to 0$. Hence, in three dimensions, the mRNA will carry a finite current, even when $d_{\alpha\beta} \to \infty$, and this asymptotic current will depend on the diffusion constant.

In Fig. 4, we plot the asymptotic current J as a function of the effective diffusion constant D_{eff}. We observe

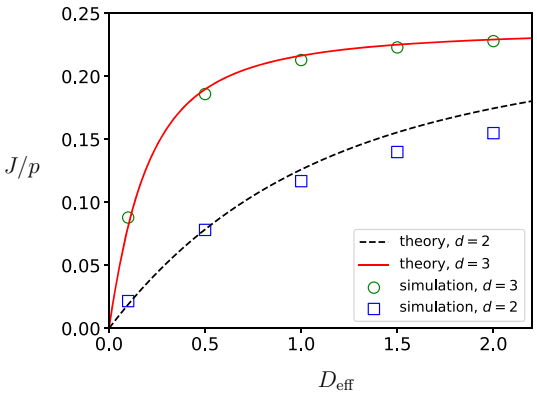

Fig. 4 Protein synthesis rate J/p as a function of the effective diffusion constant D_{eff} for filaments in $\mathbb{R}^2$ ($d = 2$) and $\mathbb{R}^3$ ($d = 3$). Analytical results from mean-field theory [lines depicting Eq. (12) with μ_d as in Eqs. (24) or (27)] are compared with simulation results (markers). The parameters used to compute the theoretical curves are $d_{\alpha\beta} = 20$, $\alpha_\infty/p = 0.4$, and $\beta/p > 1/2$ (and therefore $\lim_{D_{\text{eff}}\to\infty} J/p = 0.24$). The remaining parameters that specify the simulations can be found in Sect. 4

from Fig. 4 that at finite D_{eff} the protein synthesis rate in $d = 2$ dimensions is smaller than the synthesis rate in $d = 3$ dimensions. This is because diffusive currents are smaller in lower dimensions and hence ribosomes are more depleted at the filament entrance. For small values of D_{eff}, the current is proportional to D_{eff}, namely

$$J = \frac{\alpha_\infty}{\mu_d} D_{\text{eff}} + O(D_{\text{eff}}^2), \tag{28}$$

where the proportionality constant is the ratio between the entry rate α_∞ for circularized mRNA and the constant μ_d that depends on the geometry of the problem.

3.3.3 Two-dimensional rectangular box

Since the volume of a cell is finite, it is relevant to understand how the confinement of the mRNA in the cell affects the protein synthesis rate. We first consider the case of a filament immersed into a medium that has the shape of a two-dimensional rectangular box. This can represents a confined region of the endoplasmic reticulum membrane where translation occurs. We assume that the box is centred at the origin $\mathbf{r} = 0$ and that the sides of the box have lengths L_x and L_y.

We derive an explicit expression for the Green function in a two-dimensional rectangular box with the method of images [37]. The Green function of a point source in a two-dimensional rectangular box is identical to a series of Green functions in $\mathbb{R}^2$ associated with images of the point source, namely, it holds that

$$\mathcal{G}_{L_x,L_y}(\mathbf{r},\mathbf{r}') = \mathcal{G}_2(\mathbf{r},\mathbf{r}') + \sum_{j\in\mathcal{N}} \mathcal{G}_2(\mathbf{r},\mathbf{r}^{(j)}), \tag{29}$$

where $\mathbf{r}^{(j)}$ are the coordinates for the images of the point source located at $\mathbf{r}'$, see Fig. 5 for an example, and $\mathcal{G}_2$ is the Green function in Eq. (23).

Substituting the Green function given by Eq. (29) in Eq. (22), we obtain the expression Eq. (8), with now

$$\mu_2(L_x, L_y) = \frac{1 + \log d_{\alpha\beta} + \mathcal{I}_{L_x,L_y}}{2}, \tag{30}$$

and where $\mathcal{I}_{L_x,L_y}$ is the series

$$\mathcal{I}_{L_x,L_y} = \sum_{j\in\mathcal{N}_\beta} \log|\mathbf{r}_\alpha - \mathbf{r}_\beta^{(j)}| - \sum_{j\in\mathcal{N}_\alpha} \log|\mathbf{r}_\alpha - \mathbf{r}_\alpha^{(j)}|. \tag{31}$$

The sums in Eq. (31) run over the images of the initiation and termination sites of the filament, which define the set $\mathcal{N}_\alpha$ and $\mathcal{N}_\beta$. The specific locations of $\mathbf{r}_\alpha^{(j)}$ and $\mathbf{r}_\beta^{(j)}$ are detailed in Fig. 5. As shown in Ref. [27], the series Eq. (31) converges rapidly since the influence of the copies $\mathbf{r}_\alpha^{(j)}$ and $\mathbf{r}_\beta^{(j)}$ on the concentration of ribosomes in the original system decreases fast enough with the distance.

Note that the method of images also works for a triangular or hexagonal shaped cell as two-dimensional Euclidean space can be tiled with triangles and hexagons, see [27] and references therein.

3.3.4 Three-dimensional cuboid

Since a cell is three dimensional, we consider now the case of a three-dimensional cuboid with linear dimensions L_x, L_y and L_z. An analytical expression for the protein synthesis rate can also be derived in the case of a cuboid. We obtain formula Eq. (8) with

$$\mu_3(L_x, L_y, L_z) = \frac{2}{5} - \frac{1}{3}\left(\frac{1}{d_{\alpha\beta}} + \mathcal{I}_{L_x,L_y,L_z}\right) \tag{32}$$

where $\mathcal{I}_{L_x,L_y,L_z}$ is the series

$$\mathcal{I}_{L_x,L_y,L_z} = \sum_{j\in\mathcal{N}_\beta} \frac{r}{|\mathbf{r}_\alpha - \mathbf{r}_\beta^{(j)}|} - \sum_{j\in\mathcal{N}_\alpha} \frac{r}{|\mathbf{r}_\alpha - \mathbf{r}_\alpha^{(j)}|}. \tag{33}$$

The sums run over the images of the initiation and termination sites of the filament in $\mathbb{R}^3$.

In Fig. 6, we plot the protein synthesis rate J as a function of the height of the cuboid L_z while keeping α_∞ fixed. We observe that confinement reduces the current on the filament: the filament current in a confined volume with finite L_z is smaller than one would expect for $L_z = \infty$. In addition, we observe that the effect of confinement is negligible when $L_z > 20r$ with r the radius of the reaction volume at the first site of the filament.

It will be interesting to extend the analysis to the case of a spheroid or cylinder [38–42]. Since the main effect of confinement is a volume reduction, one can use the results for a three-dimensional cuboid to estimate the overall influence of confinement on protein synthesis rates, even for cells with a spheroid or cylindrical shape.

3.4 Summary of the theoretical results

Using a mean-field approximation, we have derived the formula (12) for the current J in the RTD model, which describes the protein translation rate for one mRNA in a diffusive reservoir that contains a large number of ribosomes. The formula Eq. (12) expresses the protein translation rate in terms of five parameters: the elongation rate p; the ratio β/p between the termination rate β and p; the ratio α_∞/p between the initiation rate α_∞ in a homogeneous reservoir, i.e. with an infinite diffusion constant D, and p; an effective diffusion constant D_{eff}; and a dimensionless parameter μ_d that quantifies the effect of the geometry of the setup on J. For small values of the parameter ζ, given by Eq. (11), we obtained the simpler expression (13), which is independent of the exit rate β and the hopping rate p.

Interestingly, all the geometrical details of the problem, such as the shape of the reservoir, the position

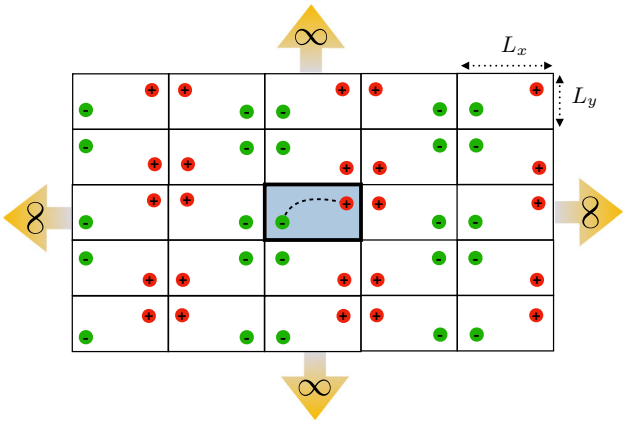

Fig. 5 Illustration of the method of images: diffusion of ribosomes in a confined rectangular box is equivalent to diffusion of ribosomes in a two-dimensional Euclidean space that contains an infinite number of images of the original source (denoted by red) and sink (denoted by green) located in the rectangular box (located in the centre and coloured in blue)

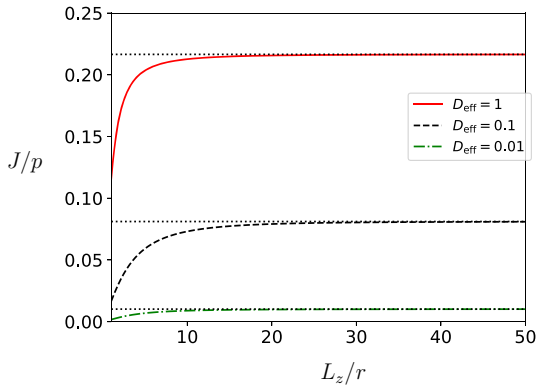

Fig. 6 Protein synthesis rate J/p as a function of L_z for filaments in a three-dimensional cuboid with $L_x = \infty$ and $L_y = \infty$. The filament is located in the x, y-plane and L_z is thus an orthogonal direction. Lines are analytical results from mean-field theory for a given value of D_{eff}. The parameters used to compute the theoretical curves are the same as in Fig. 4, namely $d_{\alpha\beta} = 20$, $\alpha_\infty/p = 0.4$, and $\beta/p > 1/2$. The dotted lines denote the asymptotics for $L_z = \infty$ and are the same as in Fig. 4

of the filament in the reservoir, and the filament end-to-end distance, are captured by the parameter μ_d. In order to understand the effect of dimensionality on μ_d, we have determined μ_d for the Euclidean spaces $\mathbb{R}^2$ and $\mathbb{R}^3$. Surprisingly, the functional dependency of μ_d on the end-to-end distance $d_{\alpha\beta}$ is qualitatively different in two than in three dimensions. In two dimensions, we find that μ_2 diverges for large $d_{\alpha\beta}$, while in three dimensions μ_3 converges to a finite value for large $d_{\alpha\beta}$. This implies that in two dimensions long mRNA filaments will have a vanishing protein translation rate, while in three dimensions the protein translation rate will be finite for long mRNA filaments. In addition, in order to understand the effect of confinement on μ_d, we have determined μ_d for a rectangle and a cuboid. Explicit computations for the cuboid show that confinement effects disappear rapidly for linear dimensions larger than $10r$, with r the size of the reaction volume.

So far, all results are based on mean-field theory. In the next section, we validate mean-field theory predictions with simulations results for the RTD model.

4 Comparing mean-field theory with simulations

We have performed numerical simulations of the RTD to verify the accuracy of the mean field theory given by Eq. (5). First, we detail the specifics of the Monte Carlo simulations. In a second subsection, we discuss the parameters used in the simulations. In a final subsection, we compare predictions from mean-field theory with simulation results.

4.1 Monte Carlo simulations of the RTD

Both components of the RTD, i.e. diffusion of particles and the active transport on the filament, can be simulated independently, using a continuous-time Monte Carlo simulation on the TASEP [43,44] and a Brownian motion in the reservoir. However, in order to simulate the RTD model, we need to couple the dynamics of the two processes.

In this subsection, we describe the algorithm used to simulate the dynamics of ribosomes in the reservoir, ribosomes on the filament, and how these two dynamics are coupled at the first and last site of the filament, where the ribosomes, respectively, enter on and exit from the filament.

First, we detail the simulations of the unbound ribosomes diffusing in the reservoir. We consider that unbound ribosomes do not interact with each other and their positions $\vec{r}$ evolve according to a Brownian equation of motion

$$\frac{d\vec{r}}{dt} = \vec{\xi}(t), \tag{34}$$

where $\vec{\xi}$ is a white noise with

$$\langle \xi_a(t) \rangle = 0, \tag{35}$$
$$\langle \xi_a(t) \cdot \xi_b(t') \rangle = 2D\delta(t - t')\delta_{a,b}, \tag{36}$$

where the indices a and b stand for the spatial coordinates of the ribosomes, i.e. x and y for a two-dimensional reservoir; and x, y and z for three-dimensional reservoir. We numerically integrate these equations by discretizing time into intervals of length $\Delta t = t - t'$, namely

$$\frac{\vec{r}(t+\Delta t)-\vec{r}(t)}{\Delta t}=\vec{\xi}(t)\,. \tag{37}$$

The $\delta(t-t')$ in the amplitude of the white noise is replaced by $1/\Delta t$, leading to the following update rule for each spatial coordinate,

$$r_a(t+\Delta t)=r_a(t)+\sqrt{2D\Delta t}\,\xi_a\,. \tag{38}$$

The reflecting boundary conditions are implemented as follows: if the update of a Brownian particle leads to a position outside of the box, the move is rejected.

Second, we detail the simulations of ribosomes bound to a filament located inside the reservoir. The filament contains ℓ sites and each site has the length $a = r$ of a ribosome. The filament has thus a total length $L = \ell r$. The dynamics on the TASEP is performed with a continuous-time Monte Carlo algorithm [43,44], sometimes called Gillespie algorithm [45,46]. A configuration of ribosomes on the filament allows only for a finite number of moves given by the TASEP rules described above. For illustration, in the particular case of Fig. 1, the first site is empty; thus, a ribosome can enter at a rate $\alpha = \tilde{\alpha}N(t)$; three ribosomes on the filament are free to move at a rate p as there is no ribosome blocking passage in front of them; and finally a ribosome occupies the exit site of the filament, so it can leave at the rate β the filament and return to the reservoir to resume a Brownian motion. It is useful to define the sum S_r of the possible transition rates; in the case of Fig. 1, $S_r = \alpha + \beta + 3p$. A particular move is chosen with a probability linearly related to its rate, and the filament is forced to perform this move. For instance, the probability P_β to move the ribosome from the exit site to the reservoir is $P_\beta = \beta/S_r$. The continuous-time Monte Carlo algorithm thus avoids rejection of ribosome moves, which saves us a considerable amount of computational time when densities of ribosomes are large. The time between two consecutive moves is a random variable τ taken from an exponential distribution with mean value like S_r^{-1}. The explicit definition of τ is important as it allows us to couple dynamics of ribosomes on the filament with the dynamics of ribosomes diffusing in the reservoir. Note that, intuitively, the sum of rates S_r, and thus the time τ spent by the filament during a move, depend on the configuration of ribosomes. If S_r is small (large), i.e. if a transition is unlikely (resp. likely) to happen, then the time evolution of the filament will be large (resp. small).

Third, we discuss how the dynamics in the reservoir is coupled to transport on the filament. First we draw a time τ from the continuous-time Monte Carlo algorithm, then we update the reservoir configuration over this time interval by integrating the Brownian equations for each particle in the reservoir over the time τ, and then we draw another time τ and so on. Hence, in this approach, we assume that in the time τ the reservoir does not change significantly. The internal dynamics of ribosome hopping is by definition not coupled to the reservoir as, in the RTD the ribosomes can neither attach nor detach in the bulk of the filament. The coupling between reservoir and filament takes place at the first and last site of the filament. Therefore, it is sufficient to define the positions $\mathbf{r}_\alpha$ and $\mathbf{r}_\beta$ of the first and the last sites, respectively. Note that the end-to-end distance $d_{\alpha\beta} = |\mathbf{r}_\beta - \mathbf{r}_\alpha|$ can take any value between 0 and L depending on the conformation of the filament. Among the possible moves accounted in the simulation is the attachment of a ribosome at the entrance: we define a spherical reaction volume $\mathcal{V}_\alpha = 4/3\pi r^3$ of radius r centred at the first site of the TASEP. If an unbound ribosome is present in the reaction volume $\mathcal{V}_\alpha$, then it can attach at a rate $\tilde{\alpha}$ to the filament, with $\tilde{\alpha}$ defined in Eq. (1). In the same way, a spherical volume V_β of radius r is centred at the exit site of the filament. If a ribosome exits the filament at a rate β, then it is released at a random position inside V_β, after which it resumes a Brownian motion in the reservoir. Note that we have used the same numerical technique in Ref. [20] to couple the TASEP-LK with Brownian particles inside a reservoir.

4.2 Parameters of the simulations

We describe in this paragraph the parameters chosen in the simulations. We first discuss the geometrical parameters. The filament has a length $L = \ell\, r$ with $\ell = 100$, which for a TASEP model is large enough to keep finite size effects of the order of a few percents [47,48]. In the simulations, the filament is located in the middle of the reservoir to ensure isotropy of the particle concentration and limiting boundary effects. The reservoir is chosen large enough with respect to $d_{\alpha,\beta}$ and r. In three dimensions, we choose the dimensions orthogonal direction to the filament equal to $L_x = L_y = 100\, r$, whereas the longitudinal direction parallel to $d_{\alpha,\beta}$ is taken to be larger, i.e. $L_z = 200\, r$. In two dimensions, we set $L_x = 400\, r$ in the longitudinal direction and $L_y = 200\, r$ in the orthogonal direction. Note that the gradient of ribosomes in the reservoir induced by the transport on the filament is expected to be larger along the longitudinal direction to $d_{\alpha,\beta}$. This is why the longitudinal dimension is chosen larger than the orthogonal directions. With these reservoir dimensions, boundary effects are small as the system is large with respect to the gradient of particles. Indeed, from Fig. 6 we can conclude that for linear dimensions larger than $20r$ the effects of confinement are negligible and the reservoir can be considered infinitely large.

We now discuss the remaining parameters of the system linked to the concentration of ribosomes, attachment rate at the entry site of the filament, and the diffusion coefficient of the Brownian motion. In three dimensions, the system contains 10^5 ribosomes, leading to a density of ribosomes $c_\infty = 0.05\, r^{-3}$, whereas in two dimensions, we set the total number of ribosomes equal to 5×10^5, leading to a density $6.25\, r^{-2}$. In two and three dimensions, we used the same parameters. We chose $\tilde{\alpha} = 0.4/c_\infty$ so that $\alpha_\infty = \tilde{\alpha}\, c_\infty = 0.4$. We chose $D = 0.1\tilde{\alpha}r^2$ and $D = \tilde{\alpha}r^2$ in Fig. 3a,b, so

that $D_{\text{eff}} = D/(\tilde{\alpha}r^2) = 0.1$ and $D_{\text{eff}} = 1$, respectively. Finally, we chose $\beta = p = 1$.

In this paragraph, we discuss the values of the correlation and equilibration times, which are important quantities to improve the sampling during Monte Carlo simulations. The correlation time can be approximated by the time needed to replace all the ribosomes on the TASEP. During one MC iteration, the time spent during the update is $\tau \sim 1/S_r \sim 1/(\rho\ell p)$ where ρ is the global density of ribosomes on the filament, i.e. $\rho = N_r/\ell$ where N_r is the total number of ribosomes on the filament. Note that, in the last approximation of τ, the sum of the rates S_r is obtained assuming that it is dominated by the hopping rates in the bulk of the TASEP, which contains $\approx \rho\ell$ particles. The last ribosome that entered the TASEP will need at least to be chosen ℓ times amongst $\rho\ell$ possibilities of moves. Therefore, the correlation time becomes $\tau_c \approx \rho\ell^2\tau = \ell/p$. As $p = 1$ and $\ell = 100$ in our simulations (both two and three dimensions), we use $\tau_c = 100$. Starting with an empty initial configuration, we ensure the steady state by performing $100\tau_c = 10^4$ iterations described above (continuous time on the filament and integration of the Brownian motion in the reservoir). Subsequently, 2×10^4 samplings are performed in three dimensions and 10^5 samplings in two dimensions, each spaced by $\tau_c = 100$ iterations to decorrelate the configurations. This leads to errors bars smaller than symbols.

4.3 Results

In Figs. 3 and 4, we compare mean-field theory with results from numerical simulations. Theory and simulations are in very good correspondence, despite the fact that theory neglects correlations between particles, finite size effects on the filament due to boundary layers, and confinement effects due to the finite volume of the reservoir. The very good correspondence between numerical experiments and theory shows that the expression for the current J given by Eqs. (10–12) describes well the effect of finite mobility on the protein synthesis rate J. In Figs. 3 and 4, we observe a small mismatch between theory and simulations regarding the protein synthesis rate at small and intermediate values of D_{eff}. We expect that these deviations are due to correlation between particles inside the reaction volume and on the filament.

5 Biological relevance of diffusion in ribosomal recycling

To determine the biological relevance of finite mobility for ribosomal recycling, we use experimentally measured values for the parameters that appear in the theoretical expression for the protein synthesis rate derived in Sect. 3. We focus on two organisms for which the required microscopic parameters have been measured experimentally, namely the bacterium *Escherichia coli* and the budding yeast *Saccharomyces cerevisiae*. Moreover, we focus on the three-dimensional case corresponding to cytoplasmic translation.

Since for physiological parameters the initiation of translation is the rate limiting step, we use the expression for the protein synthesis rate given by Eq. (13). Equation (13) implies that if

$$\mu_d \ll D_{\text{eff}} \tag{39}$$

then diffusion has no meaningful influence on the protein synthesis rate. On the other hand, when

$$\mu_d \gg D_{\text{eff}} \tag{40}$$

then the influence of finite diffusion on protein synthesis rate is sizeable. Hence, in what follows we estimate the parameters μ_d and D_{eff}.

5.1 Estimate of μ_3

First, we estimate the geometric parameter μ_3 corresponding to cytoplasmic translation. Formula (27) implies for a three dimensional and infinitely large reservoir that

$$\mu_3 \leq \frac{2}{5}, \tag{41}$$

where the equality is achieved in the limit $d_{\alpha\beta} \to \infty$.

5.2 Estimate for D_{eff} in Escherichia coli

In order to estimate D_{eff}, it is useful to rewrite the expression Eq. (9) in terms of $\langle\alpha\rangle$, which gives

$$D_{\text{eff}} = \frac{D\langle N_r\rangle}{\langle\alpha\rangle r^2} \tag{42}$$

where $\langle N_r\rangle$ is the number of ribosomes in the reaction volume. According to Eq. (A2), $\langle N_r\rangle$ is lower bounded by

$$\langle N_r\rangle > \frac{4\pi}{3}r^3 c_{\text{u}} - \frac{Jr^2}{2D} \tag{43}$$

where c_{u} denotes the concentration of unbound ribosomes. The second term in Eq. (43) is a correction due to depletion of ribosomes around the entry site. Substituting Eq. (43) in Eq. (42) and using $J = \langle\alpha\rangle$, we obtain

$$D_{\text{eff}} > \frac{4\pi}{3}\frac{Dc_{\text{u}}r}{\langle\alpha\rangle} - \frac{1}{2}. \tag{44}$$

The quantity $\langle\alpha\rangle$ is hard to estimate since it can vary in several orders of magnitude from one mRNA transcript to another, see for instance Ref. [5]. However, since initiation is the rate limiting step, it holds that

$$\langle\alpha\rangle < \frac{p}{2}, \tag{45}$$

with the elongation rate p being fairly independent of the mRNA transcript and the biological organism under study. Combining Eqs. (42) and (45), we obtain the lower bound

$$D_{\text{eff}} > \frac{8\pi}{3}\frac{Dc_{\text{u}}r}{p} - \frac{1}{2}. \tag{46}$$

We are left to estimate the parameters D, c_{u}, r and p. We first consider the case of the bacteria *Escherichia coli*.

Empirical values for the diffusion of ribosomes in *E. coli* show that $D \approx 0.04\,\mu\text{m}^2/\text{s}$, see Table 4-1 in Ref. [49]. However, the diffusion coefficient of the subunits of unbound ribosomes (i.e. those not bound to mRNA) is one order of magnitude larger and given by $D \approx 0.2\mu m^2/s$, as shown in Ref. [50].

For the radius of the reaction volume r, we use that the reaction volume cannot be smaller than the radius of a ribosome (or one of its subunits), and thus, $r >$ 10nm, see Figure 1–40 in Ref. [49].

For *E. coli*, the elongation rate p has been measured in several experiments, see Refs. [51–53], leading to a value p of about $10 - 20$ codons per second. Since a ribosome occupies three codons, we take for $p \approx 7s^{-1}$.

Lastly, we need an estimate for the concentration

$$c_{\text{u}} = \frac{N_{\text{u}}}{V}. \tag{47}$$

The volume of *E. coli* is $V \approx 1\,\mu\text{m}^3$ and its total number of ribosomes is about $N_{\text{tot}} = 20{,}000$ [49]. The fraction of unbound (or free) ribosomes is about 15% [50,54] of the total value, leading to

$$c_{\text{u}} \approx 2 \times 0.15 \times 10^4\,\mu\text{m}^{-3} \approx 3 \times 10^3\,\mu\text{m}^{-3}. \tag{48}$$

Combining all parameter values into the right hand side of the bound Eq. (46) for D_{eff}, we obtain that

$$D_{\text{eff}} > \frac{8\pi}{3}\frac{0.2 \times 10 \times 3 \times 10^3}{7}\frac{\text{nm}}{\mu\text{m}} \approx 7.2, \tag{49}$$

and therefore

$$\frac{\mu_3}{D_{\text{eff}}} < 0.06. \tag{50}$$

We can conclude that diffusion has no sizeable effect on protein synthesis rates. This is in particular true since we have been very generous with all the biological parameters. For example, taking $\langle\alpha\rangle < p/20$ instead of $p/2$, as in Ref. [55], would provide an even smaller upper bound $\frac{\mu_3}{D_{\text{eff}}} < 0.006$.

5.3 Estimate for D_{eff} in Saccharomyces cerevisiae

As a second example, we consider the case of budding yeast. We consider again Eq. (46) to bound D_{eff}. All empirical values are known for this organism, see, for instance, table S1 in Ref. [5].

Empirical values for the diffusion coefficient of the 60S subunit of ribosomes in the dense nucleoplasm of budding yeast show that $D \approx 0.3(\mu\text{m})^2/\text{s}$ [56]. We may expect that ribosomes diffuse faster in the cytoplasm, where translation takes place.

For the radius of the reaction volume r, we use again that the reaction volume cannot be smaller than the radius of the ribosome, and thus, $r >$ 10nm.

The elongation rate of ribosomes in budding yeast has been measured to be $p \sim 10$ codons per second and therefore $p \approx 3s^{-1}$ since a ribosome occupies three codons [5,57].

Finally, we come to the estimate of c_{u}, given by Eq. (47). The volume of a budding yeast cell is about $V \approx 42\mu m^3$ [5,58] and the number of ribosomes is 2×10^5 [5,59,60]. Using again that a fraction 15% of ribosomes are unbound, see Figure 3 in [5], we obtain

$$c_{\text{u}} \approx \frac{2 \times 0.15 \times 10^5}{42}\mu m^{-3} \approx 7 \times 10^3\,\mu\text{m}^{-3}, \tag{51}$$

which is in fact close to the concentration of unbound ribosomes in *E. coli*, see Eq. (48).

Combining all parameters in the bound given by Eq. (46), we obtain that

$$D_{\text{eff}} > \frac{8\pi}{3}\frac{0.3 \times 10 \times 7 \times 10^3}{3}\frac{\text{nm}}{\mu\text{m}} \approx 59 \tag{52}$$

and

$$\frac{\mu_3}{D_{\text{eff}}} < 0.007. \tag{53}$$

We should again bear in mind that the bound in Eq. (53) is a generous upper bound based on the bound on the initiation rates given by Eq. (45), and it is thus likely a loose bound and a significant overestimate for μ_3/D_{eff}.

5.4 Protein synthesis rates for E. coli

We end this section by presenting Fig. 7 that shows simulation results for the protein synthesis rate J/p in the parameter regime that is relevant for mRNA translation in *E. coli*. We compare these results from simulations with J_∞/p, the standard TASEP result for $D_{\text{eff}} = \infty$. We see that both are indistinguishable, which confirms that finite diffusion is not a limiting factor in mRNA translation.

6 Discussion

We have made a study of a totally asymmetric simple exclusion process immersed in a diffusive reservoir [11,29], which we have called the RTD model. The RTD

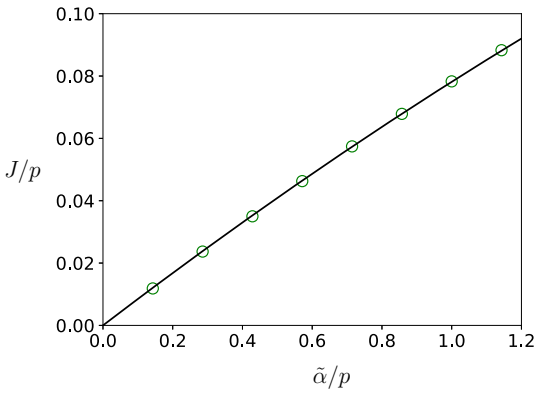

Fig. 7 We plot J/p versus $\tilde{\alpha}/p$ for biological parameters for *E. coli*: $D = 2\,\mu\text{m}^2\,\text{s}^{-1}$, $L_x = L_y = 0.7\,\mu\text{m}$ and $L_z = 2\,\mu\text{m}$ so that $V \approx 1\,\mu\text{m}^3$, $p = \beta = 7\,\text{s}^{-1}$, the radius of the reaction volume is $r = 10\,\text{nm}$, the length of the mRNA is $\ell = 300$ sites corresponding to codons, $d_{\alpha,\beta} = 300\,nm$ and we took 20.000 ribosomes in the reservoir (corresponding to the total number of ribosomes in *E. coli*). Results from simulations are given by symbols and compared to $J_\infty/p = \alpha_\infty/p(1-\alpha_\infty/p)$ corresponding to infinite diffusion constant

Table 1 Impact of finite mobilities on ribosomal recycling in two organisms

E. coli	*S. cerevisiae*
$\mu_3/D_{\text{eff}} < 0.06$	$\mu_3/D_{\text{eff}} < 0.007$

is a model for translation based on directed transport of ribosomes along mRNA and recycling of ribosomes through diffusion in the cytoplasm. We have used this model to determine whether under physiological conditions diffusion is a limiting factor for ribosome recycling.

We have derived an analytical expression for the current J at which mRNA is translated into proteins, which is corroborated by numerical simulation results. These results show that finite diffusion leads to a reduction in the translation rate J because the concentration of ribosomes at the mRNA initiation site is depleted. In addition, we find that the ratio between a geometric parameter μ_d and an effective diffusion coefficient D_{eff} determines whether diffusion has an impact on the protein synthesis rate: if $\mu_d \ll D_{\text{eff}}$, then the concentration of ribosomes at the 5' end of the mRNA is not affected by finite diffusion; on the other hand, if $\mu_d \gg D_{\text{eff}}$, then depletion of ribosomes at the mRNA initiation site is significant.

Using a broad range of physical parameters, we find that it is unlikely that finite diffusion is a limiting factor under physiological conditions in ribosome recycling. Indeed, in Table 1, we present generous upper bounds for the parameter μ_d/D_{eff} for two organisms, namely the bacterium *E. coli* and the yeast *S. cerevisiae*. In both cases, we obtain that μ_d/D_{eff} is substantially smaller than 1.

The outcome of our analysis, namely that the finite mobility of ribosomes does not play a role in translation control, is not a complete surprise given that ribosomes diffuse at large enough rates. For example, it takes 0.1 s for a protein to diffuse across an *E. coli* cell and 10 s for a protein to diffuse across a yeast cell [61], while the time to translate a protein is about 2 min [61]. Hence, as much as concerns the translation of mRNA into proteins, the diffusion rate of ribosomes can be considered very large and therefore of negligible effect on the whole translation process. Also, since ribosomes biogenesis is one of the most resource expensive processes for cells [59,62], it is reasonable to assume that the molecular conditions are optimized by evolutionary constraints in order to render translation efficient, which in the present context implies that translation is not limited by ribosome mobilities.

From a biological point of view, these results imply that the purpose of mRNA circularisation [1,9] is not the optimization of ribosome recycling by reducing the limiting factor of diffusion in the cytoplasm. Instead, the circularisation of mRNA may regulate the efficiency of translation initiation by altering the binding strength of initiation factors to the mRNA [9,10]. Hence, we come to a different conclusion than Ref. [7], which argues that three-dimensional diffusion of ribosomes in the cytoplasm plays an important role for mRNA translation control. Note that the question of the effect of the finite mobility of ribosomes on the current on mRNA remains open in two dimensions, as the diffusion coefficient of ribosomes constrained to a two-dimensional diffusion on the endoplasmic reticulum is not known to our knowledge.

Although finite diffusion is not rate limiting for ribosome recycling under physiological conditions, the RTD model may be relevant to explain the reduction in protein production when cells are in a dormant state. The mobility of cytoplasmic particles in dormant yeast cells is much lower than their mobility in yeast cells under normal conditions [63,64]. The reduction in mobility of cytoplasmic particles is due to a transition between a fluid-like phase and a solid-like phase of the cytoplasm, which is triggered by the acidification of the cytosol [64]. The formula $J \sim D$ indicates that the protein synthesis rate scales proportional to the particle mobility at low values of D.

The RTD model is also interesting as a model for the coupling between active transport and passive diffusion. Remarkably, the rate J admits a universal form that depends on five parameters only: the elongation rate p, the ratio β/p between the rate β of termination and p, the ratio α_∞/p between the initiation rate α_∞ for a homogeneous reservoir (i.e. the limit of an infinitively fast diffusion) and p, an effective diffusion constant D_{eff}, and a dimensionless parameter μ_d that quantifies the effect of the geometry of the reservoir and the filament on the current J. We have also found an interesting qualitative distinction between finite diffusion in two and three dimensions. In two dimensions, it holds that the current J vanishes in the large distance limit between the filament end-points, while in three

dimensions this limit gives a finite current J. However, the decay towards zero of J in two dimensions, which may be relevant for the endoplasmic reticulum translation, is logarithmically slow.

We end the paper by discussing the assumptions made by the RTD model and interesting future extensions of the present paper. First, we have ignored the fact that ribosomes disassemble into two subunits in the cytoplasm [1]. Hence, in principle we should consider a reservoir with two types of particles. However, if the mRNA binding rate one of these subunits is rate limiting, then the predictions of our model would remain valid. Interestingly, experimental data indicate that in prokaryotes the binding of the 40S ribosomal subunit is the rate-limiting step of initiation [4]. Second, we have assumed that mRNA has zero mobility and we have also assumed that the end-points of the mRNA are immobile. Nevertheless, including diffusion of the mRNA in the model would not alter the main conclusions of this paper, since it would only reduce the effects of finite diffusion on the protein synthesis rate. Third, it is known that cytoplasmic particles diffuse anomalously within living cells [65–67] and therefore a model based on fractional Brownian motion is more appropriate [67]. However, the exponent of the anomalous diffusion is close to 1 (0.88 for nanosilica particles of various sizes in yeast cells [64]), and therefore we expect it not to have a major impact on short length scales. It would nevertheless be interesting to analyse the dependence of J on $d_{\alpha\beta}$ in this case.

Acknowledgements This work was supported in part by a "Modélisation pour le Vivant" CNRS Grant CoilChrom (2019–2020), the project I-SITE MUSE "NMJ ON CHIP" (AAP18REC-FRM04-NMJ) and the LabEx NUMEV (ANR-10-LABX-0020) within the I-SITE MUSE of Montpellier University [No. AAP 2013-2-005, and Flagship Project Gene Expression Modeling (2017–2020)]. O.D. acknowledges doctoral thesis support from the French Ministère de l'Enseignement Supérieur, de la Recherche et de l'Innovation. A.P. acknowledges CNRS for a dispense of a semester (demi-delegation) from teaching duties.

Author contribution statement

Olivier Dauloudet, Izaak Neri and Jean-Charles Walter have contributed equally to this work.

Data availability statement This manuscript has no associated data or the data will not be deposited. [Authors' comment: This is a theoretical study without experimental data.]

Appendix A: Concentration of ribosomes in the box

We solve Eqs. (19)–(18) in various geometries when $|\mathbf{r}_\beta - \mathbf{r}_\alpha| > 2r$.

In $\mathbb{R}^2$, we obtain that

$$c(\mathbf{r}) = \begin{cases} c_\infty + \frac{Jr^2}{4D\mathcal{V}} - \frac{J}{4D\mathcal{V}}|\mathbf{r}-\mathbf{r}_\beta|^2 \\ \quad + \frac{Jr^2}{2D\mathcal{V}} \ln\left(\frac{|\mathbf{r}-\mathbf{r}_\alpha|}{r}\right), & |\mathbf{r}-\mathbf{r}_\beta| < r, \\ c_\infty - \frac{Jr^2}{4D\mathcal{V}} + \frac{J}{4D\mathcal{V}}|\mathbf{r}-\mathbf{r}_\alpha|^2 \\ \quad - \frac{Jr^2}{2D\mathcal{V}} \ln\left(\frac{|\mathbf{r}-\mathbf{r}_\beta|}{r}\right), & |\mathbf{r}-\mathbf{r}_\alpha| < r, \\ c_\infty - \frac{Jr^2}{2D\mathcal{V}} \ln\left(\frac{|\mathbf{r}-\mathbf{r}_\beta|}{|\mathbf{r}-\mathbf{r}_\alpha|}\right), & |\mathbf{r}-\mathbf{r}_\alpha| > r, \\ & \text{and } |\mathbf{r}-\mathbf{r}_\beta| > r, \end{cases} \tag{A1}$$

while in $\mathbb{R}^3$ it holds that

$$c(\mathbf{r}) = \begin{cases} c_\infty + \frac{Jr^2}{2D\mathcal{V}} - \frac{J}{6D\mathcal{V}}|\mathbf{r}-\mathbf{r}_\beta|^2 \\ \quad - \frac{Jr^3}{3D\mathcal{V}} \frac{1}{|\mathbf{r}-\mathbf{r}_\alpha|}, & |\mathbf{r}-\mathbf{r}_\beta| < r, \\ c_\infty - \frac{Jr^2}{2D\mathcal{V}} + \frac{J}{6D\mathcal{V}}|\mathbf{r}-\mathbf{r}_\alpha|^2 \\ \quad + \frac{Jr^3}{3D\mathcal{V}} \frac{1}{|\mathbf{r}-\mathbf{r}_\beta|}, & |\mathbf{r}-\mathbf{r}_\alpha| < r, \\ c_\infty + \frac{Jr^3}{3D\mathcal{V}} \left(\frac{1}{|\mathbf{r}-\mathbf{r}_\beta|} - \frac{1}{|\mathbf{r}-\mathbf{r}_\alpha|}\right), & |\mathbf{r}-\mathbf{r}_\alpha| > r, \\ & \text{and } |\mathbf{r}-\mathbf{r}_\beta| > r. \end{cases} \tag{A2}$$

For a rectangular box of dimensions $L_x \times L_y$, we obtain

$$c(\mathbf{r}) = \begin{cases} c_\infty + \frac{Jr^2}{4D\mathcal{V}} - \frac{J}{4D\mathcal{V}}|\mathbf{r}-\mathbf{r}_\beta|^2 \\ \quad + \frac{Jr^2}{2D\mathcal{V}} \ln\left(\frac{|\mathbf{r}-\mathbf{r}_\alpha|}{r}\right) + c_{\mathcal{I}}(\mathbf{r}), & |\mathbf{r}-\mathbf{r}_\beta| < r, \\ c_\infty - \frac{Jr^2}{4D\mathcal{V}} + \frac{J}{4D\mathcal{V}}|\mathbf{r}-\mathbf{r}_\alpha|^2 \\ \quad - \frac{Jr^2}{2D\mathcal{V}} \ln\left(\frac{|\mathbf{r}-\mathbf{r}_\beta|}{r}\right) + c_{\mathcal{I}}(\mathbf{r}), & |\mathbf{r}-\mathbf{r}_\alpha| < r, \\ c_\infty - \frac{Jr^2}{2D\mathcal{V}} \ln\left(\frac{|\mathbf{r}-\mathbf{r}_\beta|}{|\mathbf{r}-\mathbf{r}_\alpha|}\right) + c_{\mathcal{I}}(\mathbf{r}), & |\mathbf{r}-\mathbf{r}_\alpha| > r, \\ & \text{and } |\mathbf{r}-\mathbf{r}_\beta| > r. \end{cases} \tag{A3}$$

where

$$c_{\mathcal{I}}(\mathbf{r}) = \frac{Jr^2}{2D\mathcal{V}} \sum_{j\in\mathcal{N}_\alpha} \ln(|\mathbf{r}-\mathbf{r}_\alpha^{(j)}|) - \frac{Jr^2}{2D\mathcal{V}} \sum_{j\in\mathcal{N}_\beta} \ln(|\mathbf{r}-\mathbf{r}_\beta^{(j)}|), \tag{A4}$$

and where the $\mathbf{r}_\alpha^{(j)}$ denote the coordinates of the images of the filament initiation site located at $\mathbf{r}_\alpha$, and where the $\mathbf{r}_\beta^{(j)}$ denote the coordinates of the images of the filament termination site located at r_β, as illustrated in Fig. 5.

Analogously, for a cuboid of dimensions $L_x \times L_y \times L_z$, we obtain

$$c(\mathbf{r}) = \begin{cases} c_\infty + \frac{Jr^2}{2D\mathcal{V}} - \frac{J}{6D\mathcal{V}}|\mathbf{r}-\mathbf{r}_\beta|^2 \\ \quad - \frac{Jr^3}{3D\mathcal{V}} \frac{1}{|\mathbf{r}-\mathbf{r}_\alpha|} + c_{\mathcal{I}}(\mathbf{r}), & |\mathbf{r}-\mathbf{r}_\beta| < r, \\ c_\infty - \frac{Jr^2}{2D\mathcal{V}} + \frac{J}{6D\mathcal{V}}|\mathbf{r}-\mathbf{r}_\alpha|^2 \\ \quad + \frac{Jr^3}{3D\mathcal{V}} \frac{1}{|\mathbf{r}-\mathbf{r}_\beta|} + c_{\mathcal{I}}(\mathbf{r}), & |\mathbf{r}-\mathbf{r}_\alpha| < r, \\ c_\infty + \frac{Jr^3}{3D\mathcal{V}} \left(\frac{1}{|\mathbf{r}-\mathbf{r}_\beta|} - \frac{1}{|\mathbf{r}-\mathbf{r}_\alpha|}\right) \\ \quad + c_{\mathcal{I}}(\mathbf{r}), & |\mathbf{r}-\mathbf{r}_\alpha| > r, \\ & \text{and } |\mathbf{r}-\mathbf{r}_\beta| > r, \end{cases} \tag{A5}$$

where

$$c_{\mathcal{I}}(\mathbf{r}) = -\frac{Jr^3}{3D\mathcal{V}} \sum_{j\in\mathcal{N}_\alpha} \frac{1}{|\mathbf{r}-\mathbf{r}_\alpha^{(j)}|} + \frac{Jr^3}{3D\mathcal{V}} \sum_{j\in\mathcal{N}_\beta} \frac{1}{|\mathbf{r}-\mathbf{r}_\beta^{(j)}|}. \tag{A6}$$

References

1. H. Lodish et al., *Molecular Cell Biology*, 8th edn. (W.H. Freeman and Company, 2016)
2. M. Kosak, Initiation of translation in prokaryotes and eukaryotes. Gene **234**, 187–208 (1999)
3. T.V. Pestova et al., Molecular mechanisms of translation initiation in eukaryotes. Proc. Nat. Acad. Sci. **98**, 7029–7036 (2001)
4. J.W.B. Hershey, J.N. Sonenberg, M.B. Mathews, Principles of translational control: an overview. Cold Spring Harb. Perspect. Biol. **4**, a011528 (2012)
5. P. Shah, Y. Ding, M. Niemczyk, G. Kudla, J.B. Plotkin, Rate-limiting steps in yeast protein translation. Cell **153**, 1589–1601 (2013)
6. T. Chou, Ribosome recycling, diffusion, and mRNA loop formation in translational regulation. Biophys. J. **85**, 755–773 (2003)
7. L.D. Fernandes, P.S. De Moura, L. Ciandrini, Gene length as a regulator for ribosome recruitment and protein synthesis: theoretical insights. Scientific reports **7**, 1–11 (2017)
8. L.D. Fernandes, L. Ciandrini, Driven transport on a flexible polymer with particle recycling: A model inspired by transcription and translation. Phys. Rev. E **99**, 052409 (2019)
9. S.E. Wells, P.E. Hillner, R.D. Vale, A.B. Sachs, Circularization of mRNA by eukaryotic translation initiation factors. Mol. Cell **2**, 135–140 (1998)
10. Q. Vicens, J.S. Kieft, O.S. Rissland, Revisiting the closed-loop model and the nature of mRNA 5'-3' communication. Mol. Cell **72**, 805–812 (2018)
11. R.A. Blythe, M.R. Evans, Nonequilibrium steady states of matrix-product form: a solver's guide. J. Phys. A: Math. Theor. **40**, R333 (2007)
12. C.T. MacDonald, J.H. Gibbs, A.C. Pipkin, Kinetics of biopolymerization on nucleic acid templates. Biopolymer **6**, 1–5 (1968)
13. C.T. MacDonald, J.H. Gibbs, Concerning the kinetics of polypeptide synthesis on polyribosomes. Biopolymer **7**, 707 (1969)
14. M.C. Romano, M. Thiel, I. Stansfield, C. Grebogi, Queueing phase transition: theory of translation. Phys. Rev. Lett. **102**, 198104 (2009)
15. P. Bonnin, N. Kern, N.T. Young, I. Stansfield, M.C. Romano, Novel mRNA-specific effects of ribosome drop-off on translation rate and polysome profile. PLoS Comput. Biol. **13**, e1005555 (2017)
16. R.M. McFarland, et al., The molecular aetiology of tRNA synthetase depletion: induction of a GCN4 amino acid starvation response despite homeostatic maintenance of charged tRNA levels. Nucleic Acids Res. 48, 3071–3088 (2020)
17. R. Lipowsky, S. Klumpp, T.M. Nieuwenhuizen, Random walks of cytoskeletal motors in open and closed compartments. Phys. Rev. Lett. **87**, 108101 (2001)
18. S. Klumpp, R. Lipowsky, Traffic of molecular motors through tube-like compartments. J. Stat. Phys. **113**, 233–268 (2003)
19. M.J. Müller, S. Klumpp, R. Lipowsky, Molecular motor traffic in a half-open tube. J. Phys.: Condens. Matter **17**, S3839 (2005)
20. L. Ciandrini, I. Neri, J.C. Walter, O. Dauloudet, A. Parmeggiani, Motor protein traffic regulation by supply-demand balance of resources. Phys. Biol. **11**, 056006 (2014)
21. I. Neri, N. Kern, A. Parmeggiani, Modeling cytoskeletal traffic: an interplay between passive diffusion and active transport. Phys. Rev. Lett. **110**, 098102 (2013)
22. I. Neri, N. Kern, A. Parmeggiani, Exclusion processes on networks as models for cytoskeletal transport. New J. Phys. **15**, 085005 (2013)
23. I.R. Graf, E. Frey, Generic transport mechanisms for molecular traffic in cellular protrusions. Phys. Rev. Lett. **118**, 128101 (2017)
24. M. Rank, A. Mitra, L. Reese, S. Diez, E. Frey, Limited resources induce bistability in microtubule length regulation. Phys. Rev. Lett. **120**, 148101 (2018)
25. A.K. Verma, A.K. Gupta, Stochastic transport on flexible lattice under limited resources. J. Stat. Mech: Theory Exp. **103210** (2019)
26. A. Jindal, A.K. Verma, A.K. Gupta, Cooperative dynamics in bidirectional transport on flexible lattice (2020). arXiv:2002.09305
27. O. Dauloudet, *Étude Théorique Des Phénomènes de Transport Intracellulaire Hors-Équilibre Thermodynamique: Rôle Du Couplage Entre Transport Actif et Diffusif En*, vol. confiné (Montpellier University, PhD Diss., 2015)
28. A. Parmeggiani, *Non-Equilibrium Collective Transport on Molecular Highways, in Traffic and Granular Flow'07* (Springer, Berlin, Heidelberg, 2009), pp. 667–677
29. T. Chou, K. Mallick, R.K.P. Zia, Non-equilibrium statistical mechanics: from a paradigmatic model to biological transport. Rep. Prog. Phys. **74**, 116601 (2011)
30. D. Chowdhury, Stochastic mechano-chemical kinetics of molecular motors: a multidisciplinary enterprise from a physicist's perspective. Phys. Rep. **529**, 1–197 (2013)
31. B. Derrida, E. Domany, D. Mukamel, An exact solution of a one-dimensional asymmetric exclusion model with open boundaries. J. Stat. Phys. **69**, 667–687 (1992)
32. V.L. MacKay et al., Gene expression analyzed by high-resolution state array analysis and quantitative proteomics: response of yeast to mating pheromone. Molecular & Cellular Proteomics **3**, 478–489 (2004)
33. A. Biever et al., Monosomes actively translate synaptic mRNAs in neuronal processes. Science **367**, 6477 (2020)
34. J.L. Cook, R.K.P. Zia, Feedback and fluctuations in a totally asymmetric simple exclusion process with finite resources. J. Stat. Mech: Theory Exp. **2009**, P02012 (2009)
35. P.C. Bressloff, M. Jay, Newby, Stochastic models of intracellular transport. Rev. Mod. Phys. **85**, 135 (2013)
36. J.D. Jackson, *Classical Electrodynamics*, 3rd edn. (John Wiley & Sons, New York, 1999)
37. R.P. Feynman, R.B. Leighton, M. Sands, The Feynman Lectures on Physics: Mainly Electromagnetism and Matter **2** (1977)
38. Andrei D. Polyanin, Vladimir E. Nazaikinskii, *Handbook of Linear Partial Differential Equations for Engineers and Scientists* (CRC Press, 2015)

39. Horatio Scott Carslaw, John Conrad Jaeger, *Conduction of Heat in Solids. No. BOOK* (Clarendon press, 1992)
40. B.M. Nayar, Neumann function for the sphere. 1. Indian Journal of Pure & Applied Mathematics **12**(10), 1266–1282 (1981)
41. B.M. Nayar, Neumann function for the sphere. 2. Indian Journal of Pure & Applied Mathematics **12**(10), 1283–1292 (1981)
42. Changfeng Xue, Robert Edmiston, Shaozhong Deng, Image Theory for Neumann Functions in the Prolate Spheroidal Geometry. Advances in Mathematical Physics **2018** (2018)
43. M. Newman, G. Barkema, *Monte Carlo Methods in Statistical Physics* (Oxford University Press, New York, 1999)
44. J.-C. Walter, G.T. Barkema, An introduction to Monte Carlo methods. Physica A **418**, 78–87. Lecture Notes of the 13th International Summer School: Fundamental Problems in Statistical Physics (Leuven, Belgium, 16–29 June 2013)
45. D.T. Gillespie, A general method for numerically simulating the stochastic time evolution of coupled chemical reactions. J. Comput. Phys. **22**, 403–34 (1976)
46. D.T. Gillespie, Exact stochastic simulation of coupled chemical reactions. The Journal of Physical Chemistry **81**, 2340–61 (1977)
47. B. Derrida, E. Domany, D. Mukamel, An exact solution of a one-dimensional asymmetric exclusion model with open boundaries. J. Stat. Phys. **69** (1992)
48. A.B. Kolomeisky, G.M. Schütz, E.B. Kolomeisky, J.P. Straley, Phase diagram of one-dimensional driven lattice gases with open boundaries. J. Phys. A: Math. Gen. **31**, 6911–6919 (1998)
49. R. Milo, R. Phillips, *Cell Biology by the Numbers* (Garland Science, 2016)
50. A. Sanamrad et al., Single-particle tracking reveals that free ribosomal subunits are not excluded from the Escherichia coli nucleoid. Proc. Nat. Acad. Sci. **111**, 11413–11418 (2014)
51. R. Young, H. Bremer, Polypeptide-chain-elongation rate in Escherichia coli B/r as a function of growth rate. Biochem. J. **160**, 185–194 (1976)
52. N. Bilgin, F. Claesens, H. Pahverk, M. Ehrenberg, Kinetic properties of Escherichia coli ribosomes with altered forms of S12. J. Mol. Biol. **224**, 1011–1027 (1992)
53. S. Proshkin, A.R. Rahmouni, A. Mironov, E. Nudler, Cooperation between translating ribosomes and RNA polymerase in transcription elongation. Science **328**, 504–508 (2010)
54. J. Forchhammer, L. Lindahl, Growth rate of polypeptide chains as a function of the cell growth rate in a mutant of Escherichia coli. J. Mol. Biol. **55**, 563–568 (1971)
55. L. Ciandrini, I. Stansfield, M.C. Romano, Ribosome traffic on mRNAs maps to gene ontology: genome-wide quantification of translation initiation rates and polysome size regulation. PLoS Comput. Biol. **9**, 1 (2013)
56. J.C. Ritland Politz, R.A. Tuft, T. Pederson, Diffusion-based transport of nascent ribosomes in the nucleus. Molecular biology of the cell **14**, 4805–4812 (2003)
57. Y. Arava, Y. Wang, J.D. Storey, C.L. Liu, P.O. Brown, D. Herschlag, Genome-wide analysis of mRNA translation profiles in Saccharomyces. Proc. Natl. Acad. Sci. USA **100**, 3889–3894 (2003)
58. M. Siwiak, P. Zielenkiewicz, A comprehensive, quantitative, and genome-wide model of translation. PLoS Comput. Biol. **6**, e1000865 (2010)
59. J.R. Warner, The economics of ribosome biosynthesis in yeast. Trends Biochem. Sci. **24**, 437–440 (1999)
60. T. von der Haar, A quantitative estimation of the global translational activity in logarithmically growing yeast cells. BMC Syst. Biol. **2**, 87 (2008)
61. U. Alon, *An Introduction to Systems Biology: Design Principles of Biological Circuits* (Chapman & Hall/CRC, 2007)
62. J.L. Woolford, S.J. Baserga, Ribosome biogenesis in the yeast Saccharomyces cerevisiae. Genetics **195**, 643–681 (2013)
63. R.P. Joyner et al., A glucose-starvation response regulates the diffusion of macromolecules. Elife **5**, e09376 (2016)
64. M.C. Munder et al., A pH-driven transition of the cytoplasm from a fluid-to a solid-like state promotes entry into dormancy. Elife **5**, e09347 (2016)
65. J. Jeon et al., In vivo anomalous diffusion and weak ergodicity breaking of lipid granules. Phys. Rev. Lett. **106**, 048103 (2011)
66. V. Tejedor et al., Quantitative analysis of single particle trajectories: mean maximal excursion method. Biophys. J. **98**, 1364–1372 (2010)
67. F. Höfling, T. Franosch, Anomalous transport in the crowded world of biological cells. Rep. Prog. Phys. **76**, 046602 (2013)
68. C.U.T. Hellen, P. Sarnow, Internal ribosome entry sites in eukaryotic mRNA molecules. Genes & development **15**, 1593–1612 (2001)
69. J. Guo, X. Lian, J. Zhong, T. Wang, G. Zhang, Length-dependent translation initiation benefits the functional proteome of human cells. Mol. BioSyst. **11**, 370–378 (2015)